SAND2021-12105C

Computationally Efficient Partitioned Modeling of Inverter Dynamics with Grid Support Functions

Sunil Subedi†, Nischal Guruwacharya,
Robert Fourney, Hossein Moradi Rekabdarkolaee,
Reinaldo Tonkoski, and Timothy M. Hansen
South Dakota State University
Brookings, South Dakota, USA
Email: †sunil.subedi@jacks.sdstate.edu

Ujjwol Tamrakar
Sandia National Laboratories
Albuquerque, New Mexico, USA

Phylicia Cicilio
University of Alaska Fairbanks
Fairbanks, Alaska, USA

***Abstract*—With the advancement in power electronics technology and grid standards, traditional converters are being supplemented with the new IEEE 1547-2018 standard based grid support functions (GSFs) to support power system voltage and frequency. Inverter dynamics in power systems vary with different modes of operation, thus new modeling methods for proper system planning, operation, and dispatch are required. This work presents a data-driven approach for partitioned dynamic modeling of inverters to speed up simulation time and reduce computational complexity while ensuring acceptable accuracy. The proposed method was tested for a smart inverter with voltage support (Volt-VAr function) on a two-bus system considering dynamic residential loads, and the results showed a four-time speedup in simulation time compared to the use of the detailed model with acceptable levels of accuracy.**

***Index Terms*—Data-driven modeling, grid support functions, partitioned dynamic modeling, IEEE standard 1547-2018, simulation speedup, voltage support.**

I. Introduction

The modern power system is experiencing a rapid increase in the integration of inverter-based distributed energy resources (DERs) like photovoltaic (PV), wind, and battery energy storage systems. These power electronics (PE) converters incorporate grid support functions (GSFs) to support the voltage and frequency of the grid and to provide other ancillary services. To ease the integration and increase the penetration capacity of DERs into electric power systems, several GSFs under IEEE standard 1547-2018, such as Volt-VAr/Watt, frequency-Watt, ramp-rate control, and/or voltage/frequency ride through are in operation [1]. Contemplating the potential benefits of smart inverters with grid control settings such as active/reactive power compensation, power quality enhancement, and economic incentives, the use of such inverters is likely to increase in the future. New regulations such as IEEE 1547 with different GSFs are expected to maximize the performance of the inverters while eliminating the potential consequences that are detrimental to power system stability [2], [3]. However, integration of a high volume of PE-based smart converters can lead to technical challenges, such as dynamic instability, power quality issues, reverse power flow, and voltage and frequency fluctuations [4]. Moreover, with the integration of advanced control algorithms, the dynamic behavior of the converters while providing different ancillary services can vary significantly. Therefore, more stochastic and non-linear dynamics exist, which become a major challenge in power system stability and control [5]. It is becoming progressively important to study and accurately model PE converter-dominated power systems (CDPS) at the device level for proper system planning, operation, and dispatch while mitigating the aforementioned problems [6].

Conventional averaged linear modeling techniques become imprecise and may be computationally prohibitive in capturing all the detailed dynamic phenomena [7]. Detailed knowledge of the converter is required for the accurate non-linear modeling of its dynamics while providing different ancillary services. However, deriving detailed dynamics becomes challenging and more computationally expensive as the number of inverters increases, and the proprietary models change in their parameters, topology, and/or control strategies [8]. A generic and scalable simulation framework is required to speed up the dynamic simulation of CDPS.

The main objective of this paper is to present a general simulation framework to speed up the simulation of a CDPS and reduce computational complexity within acceptable accuracy. A black-box modeling (data-driven) approach for system identification is used in this paper, which is appropriate for modeling PE converters as it requires very little or no information about the converter's controls and topology [9]–[11]. This approach requires lower computational resources than the detailed modeling approach (e.g., switching models). However, there has been limited research in the modeling of converters equipped with advanced GSFs that have variable dynamic behavior [5]. In this work, modeling is performed via partitioning based on the operating states captured by looking at the input-output characteristics of the converters to capture the overall dynamics of the switching converter. The

This work is supported by the U.S. Department of Energy Office of Science, Office of Electricity Microgrid RD Program, and Office of Energy Efficiency and Renewable Energy Solar Energy Technology Office under the EPSCoR grant number DE-SC0020281.

The work at Sandia (Ujjwol Tamrakar) is supported by the US Department of Energy, Office of Electricity, Energy Storage Program.

Sandia National Laboratories is a multi-mission laboratory managed and operated by National Technology and Engineering Solutions of Sandia, LLC., a wholly owned subsidiary of Honeywell International, Inc., for the U.S. Department of Energy National Nuclear Security Administration under contract DE-NA-0003525. This paper describes objective technical results and analysis. Any subjective views or opinions that might be expressed in the paper do not necessarily represent the views of the U.S. Department of Energy or the United States Government.

partitioned operating ranges are represented via simpler linear models utilizing system identification tools, and the related dynamics of the converters are obtained by aggregating the piecewise linear models. To investigate the performance of the partitioned dynamic models of an inverter with advanced GSFs in practical scenarios, a two-bus model based on the 12 house benchmark model is taken from the network model of a residential neighborhood in North America presented in [12]. A dynamic load profile is used to compare both the accuracy and speed of the detailed and partitioned linearized inverter model, which shows significant improvement in the performance of the simulation.

The remainder of this paper is structured as follows: an overview of the considered advanced GSFs from IEEE standard 1547-2018 is presented in Section II. This section also includes a brief description of the proposed methodology for linearized partitioned dynamic modeling. Section III describes the details of the rural low voltage (LV) distribution benchmark model and the theoretical background of dynamic load models. In Section IV, the test system is described and followed by a discussion of the results. The main conclusions from this study are presented in Section VI.

II. GSFs and Partitioned Modeling

Generally, with LV distribution networks, power quality parameters, such as the voltage profile and voltage unbalance, are the major concerns for utilities. This section will first discuss the considered GSFs from the updated IEEE standard to regulate the voltage through reactive power in a detailed inverter model, followed by the details and importance of partitioned modeling of GSFs.

A. Reactive Power as a Function of Voltage or Volt-VAr Mode

The Volt-VAr function is intended to control inverters' reactive power output depending on the change in grid voltage. The updated IEEE standard states that, if this mode is activated, a DER shall actively control its reactive power output as a function of voltage following a Volt-VAr piece-wise linear characteristics curve as shown in Fig. 1.

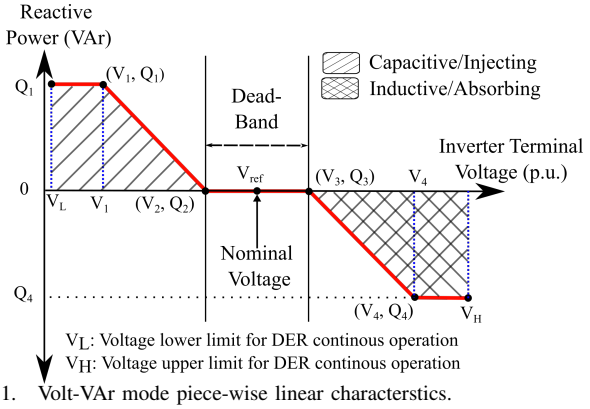

Fig. 1. Volt-VAr mode piece-wise linear characterstics.

The Volt-VAr function settings provide the shape of the curve and is defined by the change in reactive power parameters Q_1, Q_2, Q_3, and Q_4 with voltage parameters V_1, V_2, V_3, and V_4. An array of points of this Volt-VAr curve shall be configured as per the IEEE standard, or the utility's standard for the area. Referring to Fig. 1, when the inverter terminal voltage is between V_2 and V_3, the inverter's reactive power output is zero, and the region within that voltage range is called the "dead-band." If the grid voltage begins to decrease further from the lower dead-band limit of V_2, reactive power is injected into the grid, and injection is constant when the grid voltage falls below V_1. In contrast, when the grid voltage begins to exceed the upper dead-band limit of V_3, reactive power is absorbed, and constant reactive power is absorbed when the grid voltage exceeds V_4. With reference to Category "B" from the IEEE standard, voltage parameter values are 0.92, 0.98, 1.02, and 1.08 p.u for V_1, V_2, V_3, and V_4, respectively. To limit the maximum active power as a function of voltage, another important GSF, Volt-Watt (disabled by default) mode can further be used along with Volt-VAr mode to prevent the over-voltage condition.

B. Detailed Inverter Model

A single-phase grid-connected detailed inverter model system with GSFs in this study is shown in Fig. 2. The inverter is operating in current control mode, supplementing the switches. The phase-angle (θ_{PLL}) and frequency (f) of the grid are tracked with a phase-locked loop (PLL). I_f and I_{grid} are the inverter current and the current supplied to the grid, respectively. The reference active and reactive power (P^* and Q^*), respectively, are obtained either from normal operation or from the GSFs. P^* and Q^* are fed to the current reference generator, and the reference current (I^*) obtained is fed to a PI-type 2 current control loop. The inverter reference voltage is fed to the current-controlled voltage source inverter (CC-VSI). Such an inverter model requires system level detail for accurate simulation, and as the number of inverters increases, it becomes computationally expensive/intractable.

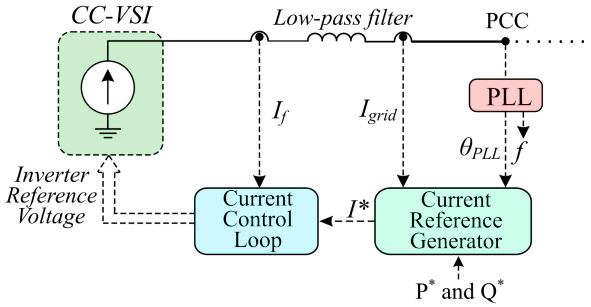

Fig. 2. Schematic diagram of the various components and control loops in a grid-connected detailed inverter system.

C. Linearized Partitioned Modeling

Modeling the aforementioned GSFs across various operating regions often results in complicated dynamic models due to the existence of non-linearities, and it is difficult to incorporate designing inverter optimal controls. The dynamics of the operating regions (within each GSF) of an inverter can be represented by computationally efficient linearized transfer function (TF) models. However, a single linearized model does not accurately capture the detailed dynamics of the entire operating region. To achieve both speed and accuracy, we

propose a partitioning linearized modeling approach where different regions of modes of operation (e.g., Volt-VAr/Watt) from the IEEE standard, are further divided into smaller ranges based on the voltage magnitude. Fig. 3 shows a conceptual diagram of partitioned linear modeling, where the droop-curve of Volt-VAr operating in different regions is partitioned into several dynamic linear TF models. This approach can also be extended to other system states as a general framework for other GSFs. Even though Fig. 3 shows linear regions, droop characteristics make the actual operation non-linear in nature. The regions are partitioned into several smaller voltage

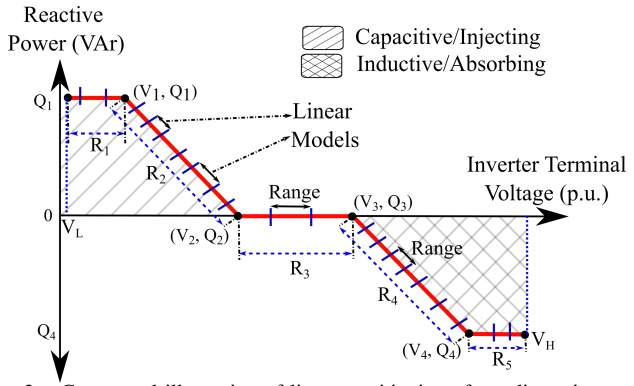

Fig. 3. Conceptual illustration of linear partitioning of non-linear inverter's mode of operation. Each region is divided into several smaller ranges with simpler linearized models.

magnitude ranges decided by looking into the input-output characteristics to develop the simpler linearized models. The flowchart of the partitioned dynamic modeling is shown in Fig. 4, where the RMS inverter terminal voltage and the inverter output current are recorded for each range. A system identification approach is applied, where the poles and zeroes are swept from a second-order to a higher-order model to form different linearized models such that it is accurate and computationally efficient. In this study, a square wave with voltage amplitude over the selected range was used for training the model. However, there are other comprehensive probing signals for this application and this will be investigated in the future. The final single TF model for each range is selected after evaluating the fit metrics that capture the dynamics of that range.

The models with different poles and zeroes are evaluated as a percentage fit as in (1), where the ratio in the equation is the Normalized Root Mean Square Error (NRMSE) [5], [13], where, $y(t)$ is the data obtained from the detailed inverter simulation model, and $\hat{y}(t)$ is the data obtained from the aggregated linear TF simulation model.

$$\text{fit} = 100 \times \left(1 - \frac{\|y(t) - \hat{y}(t)\|_2}{\|y(t) - \text{mean } y(t)\|_2}\right) \quad (1)$$

Percentage fit gives the goodness of the fit between test and reference data of identified models. Models with respective poles and zeroes are further compared with Akaike's Final Prediction Error (FPE) based on the goodness of the fit and the complexity of the model, and the most accurate model

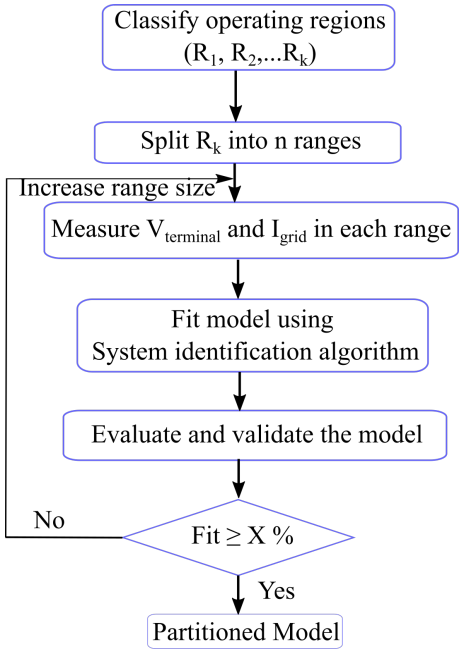

Fig. 4. Linear partitioning flowchart.

which has the lowest FPE is selected as the final TF model for each range k [5], [13]. Inverter dynamics for the entire operating region (where Volt-VAr mode activates) are obtained by aggregating all selected TFs. The performance of the aggregated linearized model compared to the detailed inverter model is evaluated by observing the recorded reactive power absorption in this study using the metrics NRMSE.

III. System Benchmark and Dynamic Load Modeling Description

For proper dynamic modeling of power systems with GSFs, North American Electric Reliability Corporation (NERC) recommends considering dynamic loads while modeling the dynamic behavior of power grids [14]–[17]. This section briefly presents the benchmark used in our dynamic study derived from the residential LV distribution network model presented in [12] with the addition of dynamic load models.

A. Dynamic Load Modeling

With technological advancements, the composition, utilization, and performance characteristics of end-use loads are continuously evolving, and load modeling is becoming more complex and important. Proper knowledge about the load and load models is crucial for power system planning, reliability, and adequate control actions to prevent system instability. Typically, load models are divided into static and dynamic, which quantify real/reactive power responses to voltage/frequency disturbances [17]. Static load models, mainly the ZIP model (constant impedance (Z), constant current (I), and constant power (P) characteristics), and the exponential load model, are widely used for steady-state simulation [18].

However, with the introduction of fast switching converter-based and more dynamic loads (e.g., induction motors (IM), air conditioners, and refrigerators), static load models become

inaccurate for voltage stability analysis [19]. Dynamic load models express the calculated powers as a function of voltage and time and are therefore necessary for the accurate analysis of both small disturbances and/or fast transient dynamics in power system simulation. In this paper, to analyze the performance of the partitioned linear dynamic models, the behavior of all static house loads is taken into account by ZIP load models, and dynamic loads are modeled as an IM.

B. Distribution Benchmark Model

Although the proposed framework is generic, this work develops a two-bus single house test system implemented in MATLAB/Simulink [1] such that it meets the characteristics of the 12^{th} house of the benchmark system, as shown in Fig. 5. A radial distribution benchmark system that consists of 12 houses, each with a grid-connected PV inverter with an installed peak capacity of 8.4 kW was presented in [12]. The houses are supplied through a 75 kVA, single-phase 14.4 kV/120-240 V distribution transformer. The detailed parameters of the benchmark feeder and the transformer are provided in [12]. Let, P and Q be the net active and reactive power injected or absorbed by a house, respectively, and R and X be the resistance and reactance of the lines, respectively. Equation (2) is used to approximate the rise or drop in the local voltage at the end of the line with respect to the beginning of the feeder [12].

$$\Delta V \approx \frac{PR + QX}{V} \tag{2}$$

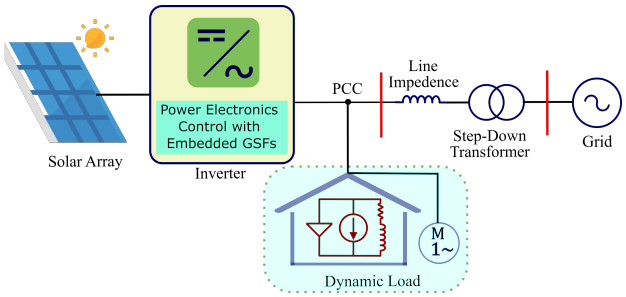

Fig. 5. Simulation framework of two-bus test system derived from 12-house benchmark system.

Net-load was varied from -8.4 kW to +8.4 kW by taking the base case with unity power factor where the inverter without GSFs is operating with a maximum output power of 8.4 kW until the terminal voltage reached 1.1 p.u. as in [12]. The magnitude of the pole-to-pole line's parameter of the test system were adjusted to match the setpoint voltage of the benchmark system while keeping the R/X ratio constant using (2). Parameters for the drop-off lines and adjusted pole-to-pole lines are summarized in the appendix in Table I.

IV. Simulation Setup

The simulation environment with the test system is briefly discussed in Subsection IV-A. To analyze the performance of the developed linear dynamic models, different input data for the available power at the PV and the dynamic residential load are described in the input load data and model subsection.

A. Test Setup for Linearized Grid Connected Inverter

For the dynamic study of the Volt-VAr mode of the inverter, a PV inverter with GSFs is connected to the residential home and assumed to supply a constant power of 70% of its maximum output power, such that net-power (PV power - load) is positive and the terminal voltage exceeds the nominal voltage. Developing the linearized TF model for Volt-VAr, the grid in Fig. 5 was replaced by a controllable voltage source and the voltage amplitude was changed in steps of 0.5 % of voltage at every 0.05 s interval for the normal operating range by keeping the frequency constant at 60 Hz. System identification provided by MATLAB/Simulink was used to develop and select the best-linearized model.

When the GSFs are activated, the inverter injects or absorbs the active or reactive power to maintain the grid voltage within the nominal operating range (i.e., 0.98 - 1.02 p.u.) following the IEEE standard 1547-2018. Both Volt-VAr and Volt-Watt mode are available for supporting the grid voltage where Volt-VAr mode activates in between $V_1 - V_2$ and $V_3 - V_4$ while the latter is enabled when the grid voltage lies in between (1.05 -1.1 p.u.).

B. Input Load Data and Load Models

The input load data for the residential house is taken from [20] using $M_t/G/\infty$ queueing model. The model stochastically creates unique load data that is statistically aggregated into a reference input load curve using freely available hourly load data from distribution companies. For this simulation, January 1, 2014, containing normal daily peak hours from the ComEd region (Chicago, IL) was used in the queueing model by scaling to a 100 W lower bound and 5000 W upper bound [20]. We have considered ZIP load models that consider both active and reactive power consumption. Based on the electric consumption of the queueing model input, a residential home with ZIP coefficients from Stratum D from [21] (provided in Table II in the appendix) and a calculated power factor of 0.96 are used. The ZIP coefficients are considered constant throughout this simulation, representing the aggregate static load characteristics of the household appliances during a particular day.

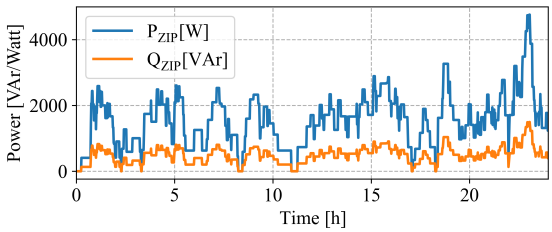

Fig. 6. Reference active and reactive power from the ZIP load model in concurrence with PV generation, IM load, and GSFs of inverter.

To add dynamics to the load profile, a single-phase asynchronous motor is connected to the house, which represents

[1]Upon acceptance, the MATLAB/Simulink model will be hosted on GitHub.

most of the motor-based household dynamic loads [22]. Detailed parameters of the motor are presented in the appendix in Table III. The ZIP load, IM load, and the PV injection are combined to serve as the reference of active and reactive power, which is fed into the house with a controlled current source. The generated reference active and reactive power from ZIP coefficients in conjunction with the house load from the queueing model, ZIP-IM load, and PV injection are shown in Fig. 6.

V. Results and Analysis

This developed linearized simulation model of the inverter is validated in this Section. Mostly, the second-order TF for each range with one zero and two poles for divided regions ($k = 5$) representing the overall dynamics of the inverter operating mode, was found to meet both accuracy and computational complexity (evaluated based on the NRMSE percentage fit and FPE metrics). In this test case, three regions (R_3, R_4, and R_5) from 0.98 - 1.08 p.u are represented by ($n = 7$) TFs. The response of the partitioned model for Volt-VAr mode was compared with the response from the detailed inverter model. To show the dynamic response of the mode under study, the IM was turned ON at 5 h, 15 h, and 20 h, which resulted in a large amount of current drawn and a sharp decrease in system voltage. With the generated load profile, the terminal voltage

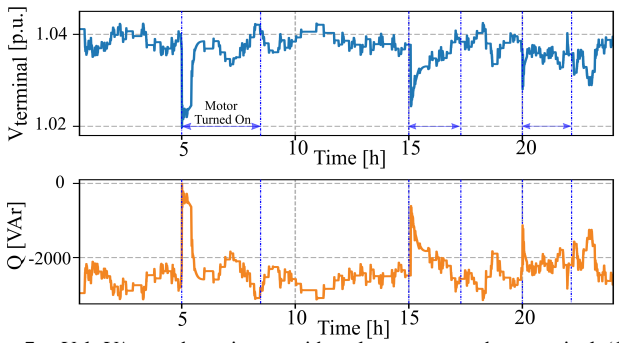

Fig. 7. Volt-VAr mode activates with voltage greater than nominal (1.02 p.u) value (top) and absorbs the reactive power from the system (bottom) to maintain the grid voltage within the nominal voltage.

in the system exceeds the upper limit of the normal operating range (i.e, 1.02 p.u.), which enables the Volt-VAr mode to first absorb reactive power from the grid as a function of voltage in the system, as shown in Fig. 7. This mode was able to reduce the terminal voltage below the over-voltage condition (V > 1.05 p.u), so there was no notable effect of the Volt-Watt mode in mitigating the over-voltage issue in this test experiment. At every instant of turning the IM ON, the grid voltage returns towards the normal operating range, and the amount of VAr absorption is decreased and results in zero absorption when the terminal voltage reaches 1.02 p.u. A significant reduction in terminal voltage from Volt-VAr mode operation was observed.

The simulation was performed on an Intel (R) Core i7 computer with 16 GB of RAM. The models were simulated in MATLAB/Simulink using the Runge Kutta 4^{th} order ODE solver with a step size of 0.1 ms. At each instant of turning on the IM, the voltage sharply dropped, and so the reactive power absorption decreased. A comparison of the amount of reactive power from the detailed inverter model and the developed linearized TF model is shown in Fig. 8. Depending on the terminal voltage, respective partitioned TFs were selected and aggregated by transitioning between them during the simulation, as shown at the bottom of Fig. 8. The NRMSE error between the overall output reactive power from the simulation of the detailed inverter model and the developed linearized TF model is just 1.91%. This shows that the developed TF model can accurately capture the dynamic behavior of the detailed system to the change in the load with an acceptable NRMSE. Along with the response from the two simulation models, the computational speed was also compared and the simulation time of the developed linearized model was faster by fourfold compared to the simulation time of the detailed inverter model. This framework shows an encouraging approach to utilities and researchers to perform larger simulations for voltage dynamic studies with a lower computational cost and acceptable accuracy as the number of inverters increases.

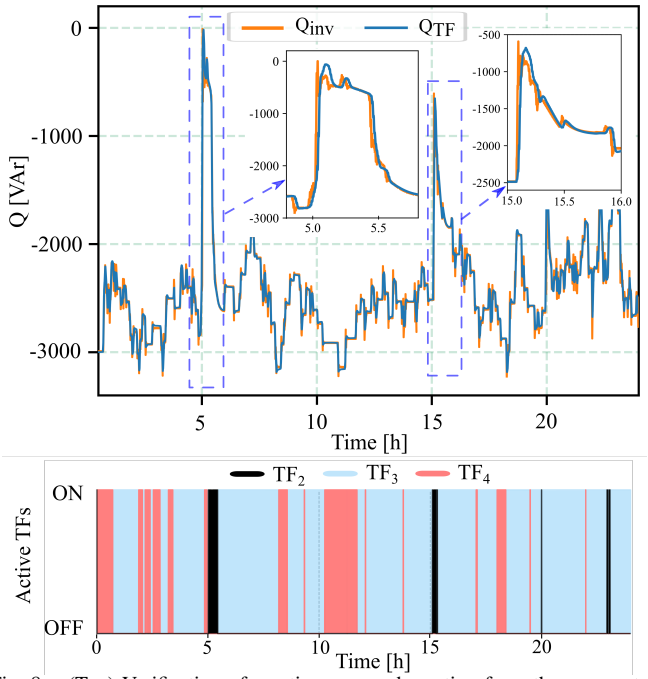

Fig. 8. (Top) Verification of reactive power absorption from the aggregated linearized model (Q_{TF}) and the actual detailed inverter model (Q_{inv}). (Bottom) Transitioning between the portioned TFs during the the simulation. Out of multiple TFs, three TFs of region R_4 in range between 1.02 and 1.05 p.u (TF_2, TF_3, and TF_4) were activated for this time period of simulation and rest TFs shall activated for other time periods.

VI. Conclusions

This paper presented a general simulated framework for the speeding up and reduction of the computational complexity of CDPS simulation. An LV distribution system network based on the 12-house benchmark system considering ZIP load, dynamic IM load, and a PV inverter with GSFs was taken as a proof of concept and modeled in MATLAB/Simulink to generate the dynamic load profile. Operating modes of the detailed inverter with GSFs were partitioned into multiple operating

ranges, and linearized TFs were developed to represent the dynamics of the PV inverter with GSFs at different voltages. It was demonstrated that combining the linearized TF models by switching between these models accurately captured the detailed non-linear dynamics of the inverter. It was also shown that the simulation speed with the developed linearized inverter model was increased fourfold compared to the detailed inverter model. These generalized TF models can be used to develop and study CDPS. Hence, the proposed framework shows the significance of allowing utilities and researchers to perform voltage dynamic large simulations with a lower computational cost and within acceptable accuracy.

ACKNOWLEDGMENTS

The authors would like to thank Alvaro Furlani Bastos from Sandia National Laboratories, Manisha Rauniyar, and Niranjan Bhujel from SDSU for reviewing the content and their valuable technical input to the paper.

REFERENCES

[1] "IEEE Standard for Interconnection and Interoperability of Distributed Energy Resources with Associated Electric Power Systems Interfaces," IEEE Std 1547-2018 (Revision of IEEE Std 1547-2003), Tech. Rep., Apr. 2018.

[2] N. Ninad, E. Apablaza-Arancibia, J. Rajda, and D. Turcotte, "Laboratory assessment of DER inverter grid support functions for updated canadian CSA C22.3 no.9 interconnection standard," in *2019 IEEE Electrical Power and Energy Conference (EPEC)*, 2019, pp. 1–6.

[3] N. Guruwacharya, N. Bhujel, T. M. Hansen, S. Suryanarayanan, R. Tonkoski, U. Tamrakar, and F. Wilches-Bernal, "Modeling inverters with grid support functions for power system dynamics studies," in *2021 IEEE Power Energy Society Innovative Smart Grid Technologies Conference (ISGT)*, 2021, pp. 1–5.

[4] S. K. Wankhede, P. Paliwal, and M. K. Kirar, "Increasing penetration of DERs in smart grid framework: A state-of-the-art review on challenges, mitigation techniques and role of smart inverters," *Journal of Circuits, Systems and Computers*, vol. 29, no. 16, p. 2030014, 2020.

[5] N. Guruwacharya, N. Bhujel, U. Tamrakar, M. Rauniyar, S. Subedi, S. E. Berg, T. M. Hansen, and R. Tonkoski, "Data-driven power electronic converter modeling for low inertia power system dynamic studies," in *2020 IEEE Power Energy Society General Meeting (PESGM)*, 2020, pp. 1–5.

[6] C. Shah, J. D. Vasquez-Plaza, D. D. Campo-Ossa, J. F. Patarroyo-Montenegro, N. Guruwacharya, N. Bhujel, R. D. Trevizan, F. A. Rengifo, M. Shirazi, R. Tonkoski, R. Wies, T. M. Hansen, and P. Cicilio, "Review of dynamic and transient modeling of power electronic converters for converter dominated power systems," *IEEE Access*, vol. 9, pp. 82 094–82 117, 2021.

[7] N. A. Ninad, D. Turcotte, and T. H. M. EL-Fouly, "Grid-interactive inverter modeling for power system studies," in *IEEE Power Energy Society General Meeting*, July 2015, 5 pp.

[8] B. Badrzadeh, Z. Emin, E. Hillberg, D. Jacobson, L. Kocewiak, G. Lietz, F. Silva, and M. val Escudero, "The need for enhanced power system modelling techniques and simulation tools," *CIGRE Science & Engineering*, vol. 17, no. February, pp. 30–46, 2020.

[9] H. Abbood and A. Benigni, "Data-driven modeling of a commercial photovoltaic microinverter," *Modelling and Simulation in Engineering*, pp. 1–11, 2018.

[10] Ju-Yeop Choi, B. H. Cho, H. F. VanLandingham, Hyung-soo Mok, and Joong-Ho Song, "System identification of power converters based on a black-box approach," *IEEE Transactions on Circuits and Systems I: Fundamental Theory and Applications*, vol. 45, no. 11, pp. 1148–1158, Nov. 1998.

[11] G. Guarderas, A. Frances, R. Asensi, and J. Uceda, "Blackbox Large-Signal Modeling of Grid-Connected DC-AC Electronic Power Converters," *Energies*, vol. 12, no. 6, 2019.

[12] R. Tonkoski, L. A. C. Lopes, and T. H. M. El-Fouly, "Coordinated active power curtailment of grid connected PV inverters for overvoltage prevention," *IEEE Transactions on Sustainable Energy*, vol. 2, no. 2, pp. 139–147, 2011.

[13] System identification toolbox. [Online]. Available: https://www.mathworks.com/help/ident/ref/fpe.html

[14] D. Dong, M. S. Agamy, M. Harfman-Todorovic, X. Liu, L. Garces, R. Zhou, and P. Cioffi, "A PV residential microinverter with grid-support function: Design, implementation, and field testing," *IEEE Transactions on Industry Applications*, vol. 54, no. 1, pp. 469–481, 2018.

[15] "NERC technical reference document, dynamic load modeling," 2016, accessed: 2021-06-06.

[16] A. Arif, Z. Wang, J. Wang, B. Mather, H. Bashualdo, and D. Zhao, "Load modeling—A review," *IEEE Transactions on Smart Grid*, vol. 9, no. 6, pp. 5986–5999, 2018.

[17] A. Faris, D. Kosterev, J. H. Eto, and D. Chassin, "Load composition analysis in support of the NERC load modeling task force 2019-2020 field test of the composite load model," Tech. Rep., 06/2020 2020.

[18] F. B. dos Reis, K. Duwadi, R. Fourney, R. Tonkoski, T. M. Hansen, M. A. I. Khan, and S. Paudyal, "Impact of residential load models for overvoltage prevention studies in PV-rich LV grids," in *2019 IEEE Milan PowerTech*, 2019, pp. 1–6.

[19] P. Cicilio, J. P. Gentle, and E. Cotilla-Sanchez, "Transient voltage stability effects on hosting capacity of behind-the-meter devices," in *2020 IEEE Power Energy Society General Meeting (PESGM)*, 2020, pp. 1–5.

[20] T. M. Hansen, E. K. P. Chong, S. Suryanarayanan, A. A. Maciejewski, and H. J. Siegel, "A partially observable markov decision process approach to residential home energy management," *IEEE Transactions on Smart Grid*, vol. 9, no. 2, pp. 1271–1281, 2018.

[21] A. Bokhari, A. Alkan, R. Dogan, M. Diaz-Aguiló, F. de León, D. Czarkowski, Z. Zabar, L. Birenbaum, A. Noel, and R. E. Uosef, "Experimental determination of the ZIP coefficients for modern residential, commercial, and industrial loads," *IEEE Transactions on Power Delivery*, vol. 29, no. 3, pp. 1372–1381, 2014.

[22] H. Ouquelle and L.-A. Dessaint, "Single-phase asynchronous machine," accessed: 20 May 2021. [Online]. Available: https://www.mathworks.com/help/physmod/sps/ug/single-phase-asynchronous-machine.html

APPENDIX

The single-phase feeder adjusted line parameters are given in Table I. Table II shows the active and reactive ZIP load coefficients for residential consumers. Single-phase IM parameters are shown in Table III.

TABLE I
SINGLE-PHASE FEEDER LINE PARAMETERS [12].

Parameters	Drop-off Lines	Pole-to-pole Lines
Resistance (Ω/km)	0.549	0.425
Inductance (mH/km)	0.23	0.294
Capacitance (μ F)	0.55	0.072

TABLE II
ACTIVE AND REACTIVE ZIP LOAD COEFFICIENTS FOR RESIDENTIAL CUSTOMERS CLASS OF STRATUM D [18], [21].

Consumer Class	Z_p	I_p	P_p	Z_q	I_q	P_q
Stratum D	1.31	-1.94	1.63	9.20	-15.27	7.07

TABLE III
SINGLE-PHASE INDUCTION MOTOR PARAMETERS [22].

	Parameters	Values
Power and Voltage	P	0.25 HP
	V	120 V
Main Winding Stator and Rotor	R_s, L_{is}	2.02 Ω, 7.4 mH
	L'_r, L'_{ir}	4.12 Ω, 5.6 mH
	L_{ms}	0.1772 H
Auxiliary Winding Stator	R_S, L_{IS}	7.14 Ω, 8.5 mH
	p	2
Capacitor-Start	R_{st}, C_s	2 Ω, 254.7 μ F
Torque and Power (used in simulation)	T, P	0.4 Nm, 0.15 kW